

Lawrence Berkeley National Laboratory

LBL Publications

Title

Determination of effective attenuation length of slow electrons in polymer films

Permalink

<https://escholarship.org/uc/item/4t5908f6>

Journal

Journal of Applied Physics, 127(24)

ISSN

0021-8979

Authors

H., J
Naulleau, P
Ahmed, M
[et al.](#)

Publication Date

2020-06-28

DOI

10.1063/5.0007163

Peer reviewed

Determination of effective attenuation length of slow electrons in polymer films

J. H. Ma,^{1,2} P. Naulleau,¹ M. Ahmed³, and O. Kostko,^{3,4, a)}

¹ Center for X-ray Optics, Lawrence Berkeley National Laboratory, Berkeley, CA 94720 (USA)

² Department of Physics, University of California, Berkeley, CA 94720 (USA)

³ Chemical Sciences Division, Lawrence Berkeley National Laboratory, Berkeley, CA 94720 (USA)

⁴ Advanced Light Source, Lawrence Berkeley National Laboratory, Berkeley, CA 94720 (USA)

a) Electronic mail: OKostko@lbl.gov

ABSTRACT

Slow electrons (with energy below 10 eV) play an important role in nature and technology. For instance, they are believed to initiate solubility change in extreme ultraviolet (EUV) resists. Depending on their mobility, such secondary electrons can lead to image blur and degradation of patterning resolution. Hence, it is important to characterize the transport of slow electrons by measuring parameters such as the effective attenuation length (EAL). We present a technique that allows for prompt characterization of EAL in polymer films. In this experiment, slow electrons are generated in a substrate upon absorption of X-ray photons. The attenuation of electron flux by a polymer film is measured as a function of the film thickness, allowing for the determination of EAL for slow electrons. We illustrate this method with poly (hydroxy styrene) and poly (methyl metacrylate) films. Furthermore, we propose an improvement for this technique that would enable the measurement of EAL as a function of electron kinetic energy.

INTRODUCTION

Slow secondary electrons are produced by all types of ionizing radiation and initiate various processes including chemical reactions. They could be used in fabrication of nanostructures and are crucial in radiation biology.¹⁻³ Another area, where low kinetic energy electrons play an important role is the field of extreme ultraviolet (EUV) lithography.⁴ Upon absorption of an EUV photon, an energetic primary electron is generated. The energy of the primary electron is deposited into the resist through inelastic scattering. While elastic scattering changes the trajectory of the electron, inelastic scattering additionally changes the energy of the electron. The electron-induced reactions, relevant to lithography, include electron impact ionization, excitation, and electron attachment.^{1,5,6} These mechanisms may result in scission of molecular bonds. Some of these processes, such as electron impact ionization or dissociative ionization, might lead to emission of secondary electrons, whereas others, like (dissociative) electron attachment, the intermolecular trapping, or solvation, will lead to removal of the interacting electron.

In EUV lithography, only a small fraction of EUV (92 eV) photons will be absorbed by a resist film. About 10-30% of EUV photons can be absorbed by a 30nm thick film, depending on film composition.⁷⁻⁹ The remaining EUV radiation will be absorbed by a substrate or an underlayer below the resist film. Absorption of an EUV photon by either of them will cause emission of a photoelectron. The emitted electron can inelastically scatter and generate several slow secondary electrons. In light of the multiplicative nature of slow electron generation, EUV resists should be tuned to capitalize the abundance of slow electrons to initiate chemical transformations which eventually lead to pattern formation. Therefore, it is very important to understand all processes initiated by electron-resist interactions as well as the length scale on which the electrons can propagate upon ionization. This length scale will ultimately define the resolution of EUV lithography.

Different techniques are used in EUV lithography to determine the role of low KE electrons in electron induced chemistry and subsequent electron induced blur. For example interaction of 80 eV electrons generated by an electron gun with a resist film and subsequent film thickness loss provides information on the distance at which electrons cause solubility changing reactions in a resist film.¹⁰ During EUV lithography numerous parameters, such as acid diffusion, secondary electron blur, and optical aberrations contribute to image blur, making it hard to extract blur length caused only by secondary electrons. Using modelling to analyze experimental results at 22 nm half pitch node it was determined that total blur length is ~4 nm. That value is dominated by acid blur and indicates that secondary electron blur should be well below that number.¹¹

For determination of the distances that electrons can travel, various direct experimental techniques (such as low energy electron transmission or photo-injection)² or Monte Carlo simulations¹² can be used. One of the direct ways to determine the effective attenuation length (EAL) in organic films is the photo-injection (also known as overlayer) technique.^{13,14} The overlayer technique is based on generation of electrons in a substrate, which is coated by an organic film. The current, proportional to the number of escaped electrons, is monitored as a function of the film thickness. This allows the determination of the film thickness at which the number of electrons is attenuated by a factor of 1/e, also known as EAL.

Many of these investigations use visible or UV light to emit valence electrons from a substrate.^{13–15} The same technique was applied to core-shell nanoparticles, where the inorganic core was used to emit electrons that penetrate through the organic shell.¹⁶

A modified version of the technique, utilizing X-ray radiation to determine EAL in polymer films is shown in Fig. 1. X-ray radiation can be tuned to maximize absorption in a silicon substrate, leaving the polymer film unchanged. Most of the electrons inside the film are injected from the silicon wafer substrate. In the absence of the resist film, electrons, generated near the surface, can freely escape to vacuum. In the presence of a resist film, the electrons will be injected into the polymer film. The injected electrons can scatter via different inelastic processes described above, leading to reduction of the number of escaped electrons. As the resist layer thickness increases, the number of electrons able to escape into vacuum decreases.

The simple cartoon in figure 1 demonstrates that the number of electrons transmitted through a polymer film decreases as the distance from the substrate-polymer interface increases. The rate of decrease is defined by electron EAL, the distance at which the original number of electrons is attenuated by a factor of $1/e$. The EAL, as well as inelastic mean free path (IMFP) – the average distance electrons travel between inelastic collisions – are also very important in surface science in general and in X-ray photoelectron spectroscopy in particular. These parameters define surface sensitivity of the technique. Hence comprehensive research of electron IMFP in different materials has been performed.^{17–20} Initially it was found that most materials, possess similar IMFP for the same electron kinetic energy (KE). Because of this similarity, the curve that outlines the dependence of IMFP as a function of electron KE is sometimes regarded as a “universal” curve.²¹ The curve displays the minimal IMFP around 0.7 nm for 20–50 eV electrons. Increase or decrease of KE from that value leads to growth of the IMFP. Thus electron with KE of 10 eV have IMFP of ~1.5 nm, 5 eV electrons can migrate on average 3 nm, whereas 1 eV electrons can travel about 100 nm between inelastic collisions.²¹ However, its universality becomes more debatable at low energies. Slow electrons are reported to have smaller IMFP values than what the “universal” curve suggests and those values are material dependent.^{22–26}

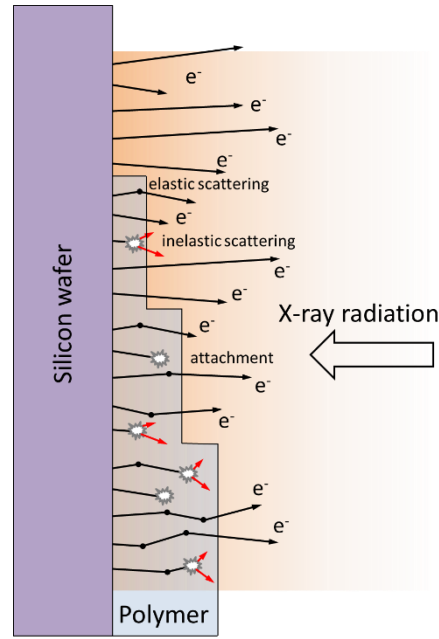


Figure 1. Scheme of the substrate-overlayer technique used to determine EAL. Absorption of X-ray photons by a silicon wafer (polymer is transparent for X-rays in this scheme) leads to electron emission from the substrate. With increase of polymer layer thickness, fewer electrons can reach the surface and escape from the polymer layer. Electrons injected in the polymer can scatter elastically, generate secondary electrons after inelastic scattering, or attach to a molecule.

To further elucidate the behavior of slow electrons, we decided to measure EAL, which defines the attenuation of the electron flux as they travel in a resist. This quantity is more applicable than IMFP to characterize image blur, because it accounts for both inelastic and elastic scattering processes, making it independent of initial and final trajectory of the electrons. EAL might be similar to IMFP if elastic scattering is weak, but for low KE electrons, elastic scattering, capable of changing electron trajectory, is prominent so EAL could be significantly smaller than IMFP.^{25,27}

A modified version of the technique is based on attenuation of substrate's soft X-ray photoelectron peaks by polymer films and leads to determination of EAL at a particular electron KE. Such experiments were conducted to determine the attenuation length of photoelectrons in self-assembled monolayers of *n*-alkanethiols.^{28,29} The hydrocarbon films of different thickness, defined by the number of monolayers, were grown on a gold substrate and attenuation of gold photoelectron peaks emitted from the substrate allowed for determination of EAL. The obtained EAL varied from 0.7 nm for KE = 50 eV up to 4.2 nm for KE = 1402 eV.^{28,29} Another study looked at how the attenuation length changes as a result of fluorination.³⁰ Despite the higher scattering cross-section of fluorine atoms the segmentally fluorinated alkanethiolate films had EALs identical to that of non-fluorinated hydrocarbon film. This was rationalized by the fact that the fluorinated segments of the film are less densely packed, therefore the net scattering properties of the fluorinated film is equal to that of hydrocarbon film with higher packing

density of weaker scattering atoms. A similar approach with a film deposited on a gold substrate was used to characterize EAL in other hydrocarbons, including PMMA³¹ or in graphene films grown on SiC substrate.³² While most of the previous research was performed using high KE electrons, for EUV lithography it would be important to investigate EAL of low KE ($KE < 80$ eV) electrons.

This paper discusses a technique developed to determine the EAL of slow electrons in polymer films. Although the method does not provide the KE dependence of the EAL, it does present an easy way to determine realistic EAL in different materials, which enables prompt resist characterization. The technique was tested using poly (hydroxy styrene) (PHS) and poly (methyl metacrylate) (PMMA), materials commonly used as the polymer matrix for resists.

EXPERIMENTAL METHODS

The electrical scheme of the experiment is shown in Fig. 2. Polymer films of different thickness are coated on Si substrates (2 in Fig. 2) and attached to a metal sample holder (1). The sample is illuminated by 200 eV photons from the Advanced Light Source (ALS) at Berkeley Lab. As will be discussed below, the photons almost entirely transmit through the thin (1 – 30 nm) films and are absorbed by the Si substrate. The substrate emits electrons with a continuous distribution dominated by low KE electrons. The electrons penetrate through the film and are collected by the positively-biased ring electrode, which is parallel to the sample surface (3). The current generated by the escaped electrons is detected by an ammeter (5). To reduce sample damage and rate of surface charging interfering with the results, the sample stage (1) is moving during the measurement. The current values are measured continuously during the sample movement, allowing for current collection from a fresh, unexposed sample area. The experimental setup is located inside of a vacuum chamber, kept at pressure below 10^{-6} Torr during measurement. The chamber is directly connected to a beamline which delivers X-ray radiation.

Thin film samples of PHS and PMMA of different thickness are prepared by spin coating polymer solutions in propylene glycol methyl ether acetate on 100 mm silicon wafers. For each thickness, a different wafer is used. The spin coated wafers are baked for 60 s at 130 C and then cleaved into 10 by 15 mm chips, used for measurement. Thickness of so prepared films is determined by a J.A. Woollam Co. M-2000 spectroscopic ellipsometer.

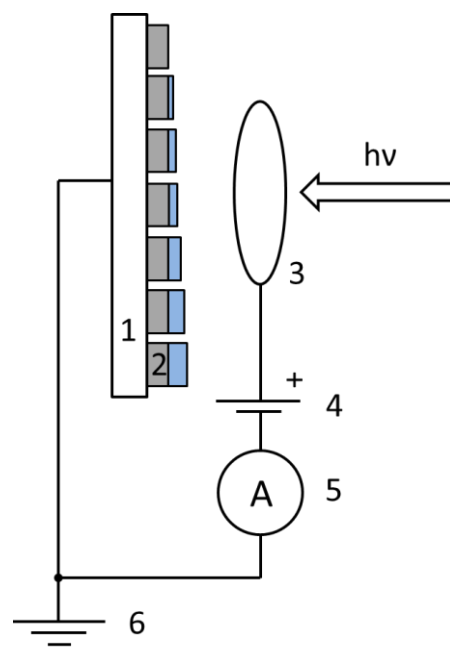


Figure 2. Electrical scheme of the experiment. (1) Metal sample holder with seven silicon wafer chips (2) coated by polymer films of various thickness. (3) Ring electrode collecting emitted electrons. (4) Positive bias between the ring and ammeter (5). (6) Ground. $h\nu$ denotes X-ray beam.

RESULTS AND DISCUSSION

We hypothesize that the experimental technique is sensitive to the electrons emitted from the substrate. To achieve that, the energy of X-ray radiation was chosen so that polymers (usually consisting of carbon, hydrogen, and oxygen) are mostly transparent, whereas the substrate efficiently absorbs the X-ray photons. EUV resists may absorb a significant fraction of EUV photons, making EUV photon energy not optimal for this measurement. Indeed, the photoabsorption cross-section of carbon at the EUV energy is about two times higher than that of silicon (see Table 1),³³ meaning that a significant fraction of EUV radiation will be absorbed in the polymer film, significantly complicating the analysis. The situation is drastically different at photon energy of 200 eV. The photo-absorption cross-sections of hydrocarbon materials are small, whereas the cross-section of silicon is large (Table 1) because the photon energy is above Si 2p edge. In this case most of the 200 eV photons will pass through the thin polymer film and will be promptly absorbed by the silicon substrate. Half of the photons reaching the surface of silicon will be absorbed in the first 44 nm of the substrate.

Table 1. Photo-absorption cross-section of carbon, oxygen, hydrogen, and silicon at photon energies of 92 eV and 200 eV.

Element	Cross-section at 92 eV, Mb	Cross-section at 200 eV, Mb
Carbon	0.58	0.10
Oxygen	2.10	0.38

Hydrogen	0.02	0.002
Silicon	0.34	3.13

To demonstrate the applicability of the technique, PHS (C_8H_8O) and PMMA ($C_5H_8O_2$) were chosen as polymer samples. Their properties at 92 eV and 200 eV are summarized in Table 2. The amount of photons absorbed by a 30 nm film is drastically different at those energies. Thus, at 92 eV both PHS and PMMA films absorb 11.5-14.6 % of EUV photons, while at 200 eV they absorb only 2.1-2.7 % of photons, depending on the material. The remaining 97 % of 200 eV radiation is absorbed by the silicon substrate.

Table 2. Absorption cross-sections of PHS and PMMA, as well as fractions of absorbed radiation by 30 nm film of these materials at photon energies of 92 eV and 200 eV.

Polymer	Cross-section at 92 eV, Mb	Cross-section at 200 eV, Mb	Absorbed 92 eV radiation, %	Absorbed 200 eV radiation, %
PHS	7.02	1.21	11.5	2.1
PMMA	7.37	1.29	14.6	2.7

After absorption of the 200 eV photon, most of the electrons emitted by the substrate are low KE secondary electrons. This is a known experimental fact observed in a range of different materials.³⁴⁻³⁷ We measured photoelectron spectra of bare silicon substrate using a retarding field photoelectron spectrometer to demonstrate the presence of slow secondary electrons. The spectra measured at photon energy of 200 eV and 92 eV are shown in Fig. 3a and b, correspondingly. Both spectra illustrate that most of the electrons emitted by a silicon wafer have a continuous distribution dominated by slow electrons, peaking around 2 eV. A similar distribution was observed by Henke et al. for different semiconductors and insulators.³⁵ The origin of the observed electron distribution is explained as follows: the absorption of a photon leads to emission of a photo- and, plausibly, an Auger electron. These electrons may scatter inelastically (via electron impact ionization process), loose part of their initial KE and generate additional low KE electrons. Several of such inelastic scattering events will decrease the initial KE of photoelectrons to a minimum, observed in the experimental spectra. Henke et al. developed a model, characterizing the shape of the SE distribution:

$$I(E_K) = k \frac{E_K}{(E_K + E_A)^3}, \quad (1)$$

where I is the energy dependent intensity, k is a fitting coefficient, E_K is electron kinetic energy, and E_A is the electron affinity. The experimental spectra are fit to the model and the results are shown in figure 3 by red lines. While the fit is not perfect, the model works well to predict that majority of emitted electrons will be the slow secondary electrons.

This is the author's peer reviewed, accepted manuscript. However, the online version of record will be different from this version once it has been copyedited and typeset.
PLEASE CITE THIS ARTICLE AS DOI: 10.1063/5.0007163

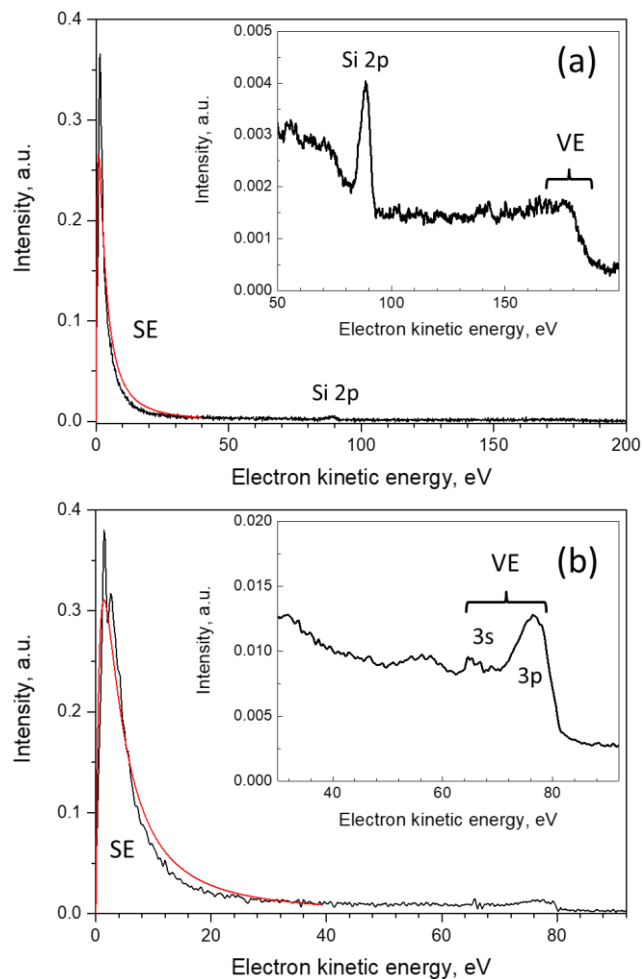


Figure 3. X-ray photoelectron spectra of silicon wafer collected at photon energy of (a) 200 eV and (b) 92 eV. Insets demonstrate the scaled up high KE electron signal. Red lines depict fit of low KE secondary electron signal with equation (1). SE: secondary electrons, VE: valence electrons.

Figure 3 also contains a weak signal generated by high KE electrons. While Si valence electrons (3s and 3p) are not resolved at 200 eV (Fig. 3a) they are slightly visible at 92 eV (Fig. 3b).^{38,39} The photoelectron spectrum measured at photon energy of 200 eV also demonstrates a Si 2p photoelectron peak around KE of 90 eV. The Si 2p peak is relatively sharp because the electrons originate from a core level of Si. It is instructive to compare the number of low KE electrons to that of high KE electrons. At photon energy of 200 eV, the low KE electrons (with KE < 20 eV) comprise 71 % of all emitted electrons, whereas at 92 eV they comprise 81 %. Similar distribution of electrons will be observed in a polymer film after absorption of EUV photons and it represents a typical electron energy distribution after several inelastic collisions. Therefore, the continuous electron distribution of low KE electrons, emitted by Si substrate after absorption of 200 eV photons can be used to characterize the EAL of polymer films.

This is the author's peer reviewed, accepted manuscript. However, the online version of record will be different from this version once it has been copyedited and typeset.

PLEASE CITE THIS ARTICLE AS DOI: 10.1063/5.0007163

Example of the data collected using the designed experimental scheme (Fig. 2) is shown in Fig. 4a. The data, collected for PHS films of six different thicknesses and a bare Si substrate, have a step-like structure, where regions of constant signal intensity correspond to electron emission from samples. Current spikes between samples are due to electron emission from the metal sample holder. It is apparent that the current emitted by a clean Si substrate has the largest value among all data points. This happens because PHS film of any thickness will attenuate the number of electrons emitted by a Si substrate. As the thickness of the film increases, the number of transmitted electrons becomes smaller. That is apparent in Fig. 4a: the 3.3 nm thick film significantly attenuates the number of electrons emitted by a Si wafer; after transmission through the film, the current diminishes from 4.9 to 2.3. An increase in the PHS film thickness to 5.1 nm further diminishes the current to 1.1. The PHS film thickness above 7.7 nm does not cause significant change, with the current converging to the value of 0.6.

This is the author's peer reviewed, accepted manuscript. However, the online version of record will be different from this version once it has been copyedited and typeset.
PLEASE CITE THIS ARTICLE AS DOI: 10.1063/5.0007163

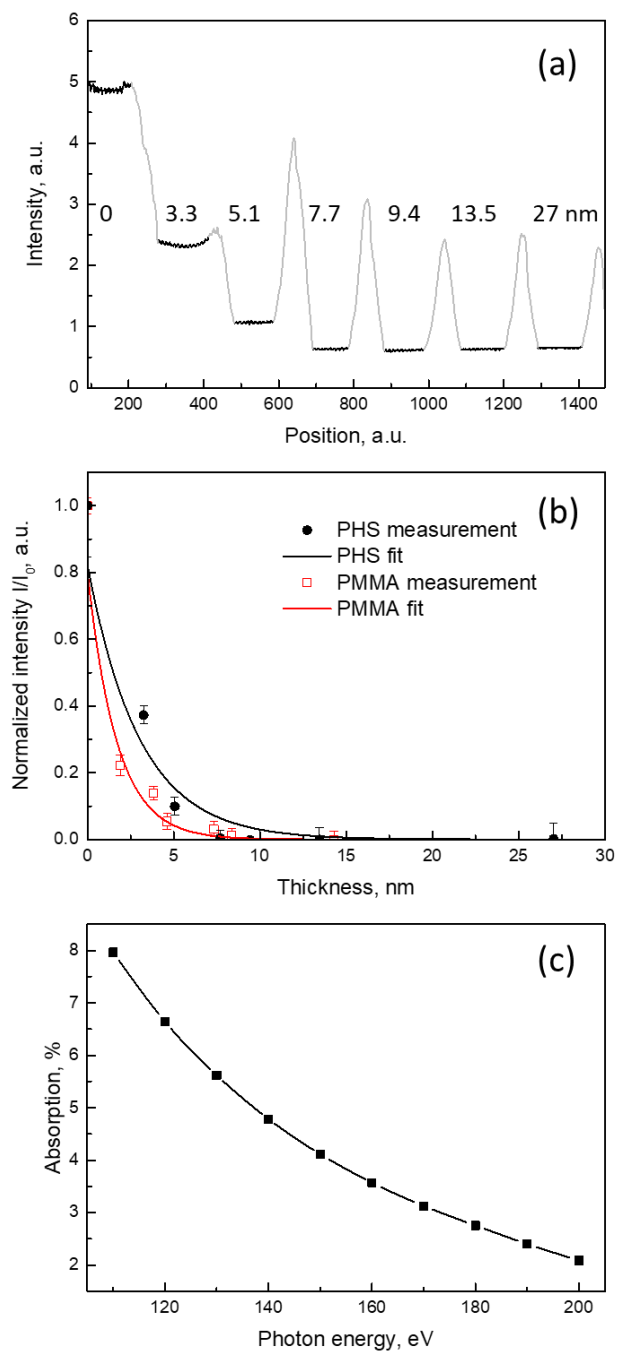


Figure 4. (a) Electron yield measurement as a function of sample position. Signal, originated from PHS films of different thickness (shown in black), is labeled with the corresponding thickness. Current spikes (shown in gray) between samples are due to electron emission from the metal sample holder. (b) Normalized electron yield for PHS and PMMA (black and red symbols) fit with exponential decay functions (black and red lines). Error bars are determined from intensity variations between five consecutive measurements. (c) Fraction of X-ray radiation absorbed by a 30 nm film of PHS.

Analysis of the electron yield determined as demonstrated in Fig. 4a is presented in Fig. 4b (black symbols and line). The normalized values of the collected current are plotted as a function of polymer thickness. The obtained experimental data are fit with the exponential decay function:

$$I(h) = I_0 \exp(-h/EAL), \quad (2)$$

where I_0 is electron current collected from a bare Si substrate, h is the thickness of a film and EAL is effective attenuation length. It is important to note that in the presence of the potential barrier at the interface between the substrate and polymer film, some electrons might be reflected back into the substrate. This accounts for a reduction of I_0 by 19% calculated via a model that solves the Schrodinger equation with a step function potential term and is described in Supplementary Information (SI). The fit of the experimental data presented in Fig. 4b results in a value of EAL for PHS of 3.10 ± 0.41 nm. This value corresponds to the thickness of PHS film that reduces the initial number of emitted slow electrons by a factor of $1/e$ (to about 37% of initial number). The corresponding data for PMMA is shown in Fig. 4b by red squares and line. Corresponding EAL for PMMA is 1.78 ± 0.17 nm.

In the context of lithography, it is important to know the thermalization distances of electrons – the distance which an electron can travel until it loses most of its energy. For PHS, the thermalization distance of 3.2 ± 0.6 nm was determined by fitting results of Monte Carlo simulation into the experimental quantum efficiency data.⁴⁰ The EAL value obtained in the current study for PHS of 3.10 ± 0.41 nm is close to the semi-empirical thermalization distance value of 3.2 ± 0.6 nm. While the EAL value defines the distance at which the population of electrons decreases to 37% ($1/e$) of the injected population, the thermalization distance can be a bit larger, because extra travel might be needed to decrease energy of electrons to the thermal level. The same authors assumed that the thermalization distance in PMMA is 6 ± 1 nm solely based on the fact that the thermalization distance in many alkane solutions ranges from 5 to 7 nm.^{41,42} Whereas the experimental study of PMMA film thickness loss caused by interaction with 80 eV electrons suggests that the electron blur for PMMA is 1.8 ± 0.2 nm.¹⁰ The latter value has similar meaning to the attenuation length and lies within the error bars of determined in this study EAL value of 1.78 ± 0.17 nm.

From formula (2), the EAL value extracted from the measurements strongly depends on knowledge of film thickness. Systematic overestimation (or underestimation) of film thickness will lead to correspondingly larger (or smaller) values of EAL . Incorrect thickness measurement of thin ($h < 3 EAL$) films might lead to significant error in EAL analysis. As it is demonstrated in the SI the potential barrier created by the substrate-film interface reduces number of electrons entering the thin film. Such reduction could be significant for low KE electrons and needs to be accounted for. If one uses only data obtained from substrates coated by films of finite thicknesses, then the substrate-film interface is involved in all experimental data points. In that case, the fractional loss in intensity resulted from barrier reflection will be identical in all data points and the reflection would not affect the extracted value of EAL . This approach should be used when feasible, although difficulties, associated with preparation of multiple films of known thickness may limit its applicability.

Because of the choice of X-ray photon energy described above, the absorption of photons by a film is negligible and might be neglected in the analysis (in the case of PHS consideration of photon

absorption decreases the EAL value by less than 0.5%). Nevertheless, the more explicit analysis, which is only possible if the composition of the polymer is known, is presented below. To account for the fraction of photons absorbed in a polymer layer, the right hand side of equation (2) should be multiplied by $(2 - \exp(-\sigma\rho h))$, where the exponential part accounts for the Beer-Lambert law (attenuation of light in the material), where σ is absorption cross-section of polymer units and ρ is number density of the polymer units. The absorption cross-section can be calculated using tabulated values of elemental cross-sections.³³

While the technique described above provides general information on behavior of slow electrons, a more detailed analysis is required in some cases, such as EAL for electrons of a particular KE. A small modification of the proposed experiment allows for determination of KE dependence of EAL. Using tunable X-ray radiation one can selectively change the KE of emitted photoelectrons. In particular, change of X-ray photon energy will lead to emission of Si 2p electrons (narrow peak in Fig. 3a) at different KE. Thus, at photon energy of 200 eV, the KE of Si 2p is 90 eV. Decrease of photon energy to 150 eV will lead to decrease of KE of emitted Si 2p electrons to 40 eV. Framing it differently, tuning the photon energy from 110 eV to 200 eV will generate Si 2p electrons with KE from 0 to 90 eV. It is worth noting that as the photon energy is decreased from 200 eV, the higher fraction of X-ray radiation will be absorbed by a polymer film. Thus, 30 nm film of PHS will absorb 4.1% of 150 eV photons and absorption reaches 8.0% at photon energy of 110 eV (Fig. 4c). This number needs to be accounted for during the data analysis as described above, because only the photons, reaching the surface of silicon can lead to emission of Si 2p electrons. A similar type of measurement as performed above, but in this case evaluating attenuation of Si 2p peak intensity as a function of polymer film thickness, can provide information on EAL of electrons with selected KE. An electron energy analyzer is needed to perform this measurement. Because high energy resolution is not required, a simple energy analyzer, such as a retarding field analyzer, can be utilized. As a result of such measurements, an EAL dependence on electron KE can be determined. The dependence will provide more information on EAL of low KE electrons and their correlation with the “universal curve”.

CONCLUSIONS

This study describes an approach to collect information on electron EAL in polymer films of interest for EUV lithography applications. The technique uses a Si substrate irradiated by X-rays to generate a continuous distribution of slow (with energy below 10 eV) secondary electrons. The photon energy is chosen so that it is almost entirely transmitted by a polymer film and is absorbed by the substrate. The generated slow electrons escape from the sample and the dependence of the resulting current as a function of film thickness allows for extraction of EAL. The EAL values of 3.10 ± 0.41 nm and 1.78 ± 0.17 nm are determined for poly (hydroxy styrene) and poly (methyl metacrylate), correspondingly. The obtained values are close to the literature values of electron thermalization length and secondary electron blur. Finally, a technique, allowing for determination of electron energy-dependent EAL values is discussed.

SUPPLEMENTARY MATERIAL

See Supplementary Material for modelling of electron reflection by a potential barrier at the interface between the substrate and polymer film.

ACKNOWLEDGEMENTS

This work is supported by the Condensed Phase and Interfacial Molecular Science Program, in the Chemical Sciences Geosciences and Biosciences Division of the Office of Basic Energy Sciences of the U.S. Department of Energy under Contract No. DE-AC02-05CH11231. This research used resources of the Advanced Light Source, which is a DOE Office of Science User Facility under Contract No. DE-AC02-05CH11231. Jonathan H. Ma is supported by C-DEN (Center for design-enable nanofabrication), member companies ASML, Carl Zeiss Group, Intel, KLA-Tencor, Mentor Graphics, and Samsung.

DATA AVAILABILITY STATEMENT

The data that support the findings of this study are available from the corresponding author upon reasonable request.

REFERENCES

- ¹ C.R. Arumainayagam, H.-L. Lee, R.B. Nelson, D.R. Haines, and R.P. Gunawardane, *Surf. Sci. Rep.* **65**, 1 (2010).
- ² R. Naaman and L. Sanche, *Chem. Rev.* **107**, 1553 (2007).
- ³ Y. Zheng and L. Sanche, *Appl. Phys. Rev.* **5**, 021302 (2018).
- ⁴ J. Torok, R.D. Re, H. Herbol, S. Das, I. Bocharova, A. Paolucci, L.E. Ocola, C.V. Jr, E. Lifshin, G. Denbeaux, and R.L. Brainard, *J. Photopolym. Sci. Technol.* **26**, 625 (2013).
- ⁵ W.F. van Dorp, in *Front. Nanosci.*, edited by A. Robinson and R. Lawson (Elsevier, 2016), pp. 115–133.
- ⁶ O. Kostko, B. Xu, M. Ahmed, D.S. Slaughter, D.F. Ogletree, K.D. Closser, D.G. Prendergast, P. Naulleau, D.L. Olynick, P.D. Ashby, Y. Liu, W.D. Hinsberg, and G.M. Wallraff, *J. Chem. Phys.* **149**, 154305 (2018).
- ⁷ S. Irie, M. Endo, M. Sasago, N. Kandaka, H. Kondo, and K. Murakami, *Jpn. J. Appl. Phys.* **41**, 4027 (2002).
- ⁸ Y. Fukushima, T. Watanabe, T. Harada, and H. Kinoshita, *J. Photopolym. Sci. Technol.* **22**, 85 (2009).
- ⁹ D.F. Ogletree, *Front. Nanosci.* **11**, 91 (2016).
- ¹⁰ S. Grzeskowiak, R.L. Brainard, and G.H. Denbeaux, in *Adv. Patterning Mater. Process. XXXVI* (International Society for Optics and Photonics, 2019), p. 1096007.
- ¹¹ R. Gronheid, T.R. Younkin, M.J. Leeson, C. Fonseca, J.S. Hooge, K. Nafus, J.J. Biafore, and M.D. Smith, in *Extreme Ultrav. EUV Lithogr. II* (International Society for Optics and Photonics, 2011), p. 796904.
- ¹² A. Jablonski and C.J. Powell, *J. Electron Spectrosc. Relat. Phenom.* **100**, 137 (1999).
- ¹³ Y.C. Chang and W.B. Berry, *J. Chem. Phys.* **61**, 2727 (1974).
- ¹⁴ S. Hino, N. Sato, and H. Inokuchi, *J. Chem. Phys.* **67**, 4139 (1977).
- ¹⁵ F.C. Marques and J.J. Jasieniak, *Appl. Surf. Sci.* **422**, 504 (2017).
- ¹⁶ M.I. Jacobs, O. Kostko, M. Ahmed, and K.R. Wilson, *Phys. Chem. Chem. Phys.* **19**, 13372 (2017).
- ¹⁷ C.J. Powell, *Surf. Sci.* **44**, 29 (1974).
- ¹⁸ I. Lindau and W.E. Spicer, *J. Electron Spectrosc. Relat. Phenom.* **3**, 409 (1974).

This is the author's peer reviewed, accepted manuscript. However, the online version of record will be different from this version once it has been copyedited and typeset.
PLEASE CITE THIS ARTICLE AS DOI: 10.1063/1.50007163

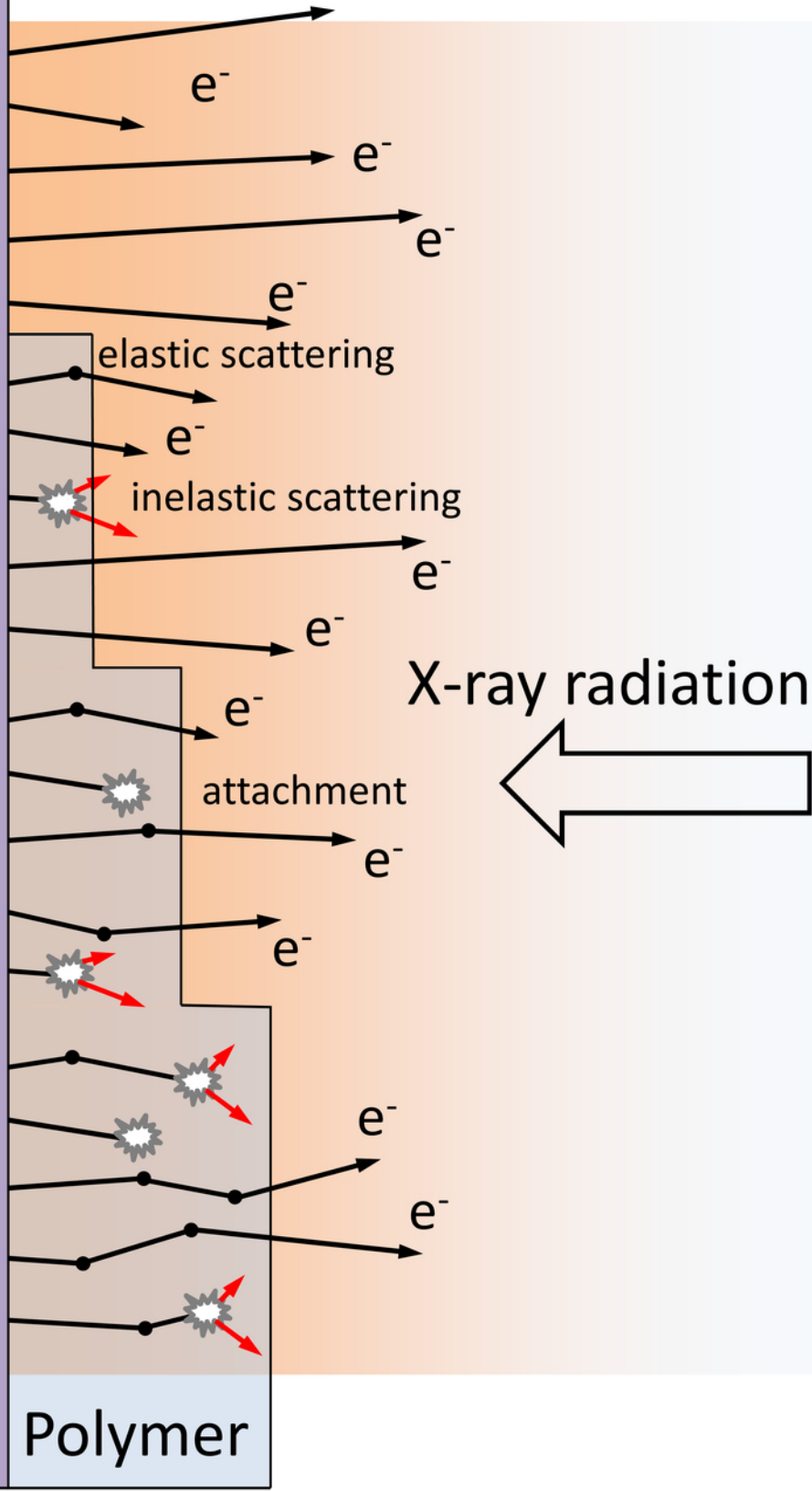
- ¹⁹ C. Martin, E.T. Arakawa, T.A. Callcott, and J.C. Ashley, *J. Electron Spectrosc. Relat. Phenom.* **35**, 307 (1985).
- ²⁰ E. Cartier and P. Pfluger, *Phys. Rev. B* **34**, 8822 (1986).
- ²¹ M.P. Seah and W.A. Dench, *Surf. Interface Anal.* **1**, 2 (1979).
- ²² D. Geelen, J. Jobst, E.E. Krasovskii, S.J. van der Molen, and R.M. Tromp, *Phys. Rev. Lett.* **123**, 086802 (2019).
- ²³ M. Michaud, A. Wen, and L. Sanche, *Radiat. Res.* **159**, 3 (2003).
- ²⁴ Y. Ozawa, Y. Nakayama, S. Machida, H. Kinjo, and H. Ishii, *J. Electron Spectrosc. Relat. Phenom.* **197**, 17 (2014).
- ²⁵ S. Thürmer, R. Seidel, M. Faubel, W. Eberhardt, J.C. Hemminger, S.E. Bradforth, and B. Winter, *Phys. Rev. Lett.* **111**, 173005 (2013).
- ²⁶ Y.-I. Suzuki, K. Nishizawa, N. Kurahashi, and T. Suzuki, *Phys. Rev. E* **90**, 010302 (2014).
- ²⁷ O. Kostko, M.I. Jacobs, B. Xu, K.R. Wilson, and M. Ahmed, *J. Chem. Phys.* **151**, 184702 (2019).
- ²⁸ C.D. Bain and G.M. Whitesides, *J. Phys. Chem.* **93**, 1670 (1989).
- ²⁹ C.L.A. Lamont and J. Wilkes, *Langmuir* **15**, 2037 (1999).
- ³⁰ R. Colorado and T.R. Lee, *J. Phys. Chem. B* **107**, 10216 (2003).
- ³¹ M.P. Seah and S.J. Spencer, *Surf. Interface Anal.* **43**, 744 (2011).
- ³² M. Amjadipour, J. MacLeod, J. Lipton-Duffin, A. Tadich, J.J. Boeckl, F. Iacopi, and N. Motta, *Nanotechnology* **30**, 025704 (2018).
- ³³ B.L. Henke, E.M. Gullikson, and J.C. Davis, *At. Data Nucl. Data Tables* **54**, 181 (1993).
- ³⁴ B.L. Henke, J.A. Smith, and D.T. Attwood, *J. Appl. Phys.* **48**, 1852 (1977).
- ³⁵ B.L. Henke, J. Liesegang, and S.D. Smith, *Phys. Rev. B* **19**, 3004 (1979).
- ³⁶ A. Ausmees, M. Elango, E. Nömmiste, J.N. Andersen, R. Nyholm, and I. Martinson, *Nucl. Instrum. Methods Phys. Res. Sect. Accel. Spectrometers Detect. Assoc. Equip.* **308**, 219 (1991).
- ³⁷ J.J. Scholtz, D. Dijkkamp, and R.W.A. Schmitz, *Philips J. Res.* **50**, 375 (1996).
- ³⁸ G. Gantner, H.G. Boyen, and P. Oelhafen, *Europhys. Lett. EPL* **31**, 163 (1995).
- ³⁹ J.D. Joannopoulos and M.L. Cohen, *Phys. Rev. B* **7**, 2644 (1973).
- ⁴⁰ T. Kozawa and S. Tagawa, *Jpn. J. Appl. Phys.* **50**, 030209 (2011).
- ⁴¹ T. Kozawa, S. Tagawa, T. Kai, and T. Shimokawa, *J. Photopolym. Sci. Technol.* **20**, 577 (2007).
- ⁴² J.-P. Jay-Gerin, T. Goulet, and I. Billard, *Can. J. Chem.* **71**, 287 (1993).

This is the author's peer-reviewed, accepted manuscript. However, the online version of record will be different from this version once it has been corrected and proofread.

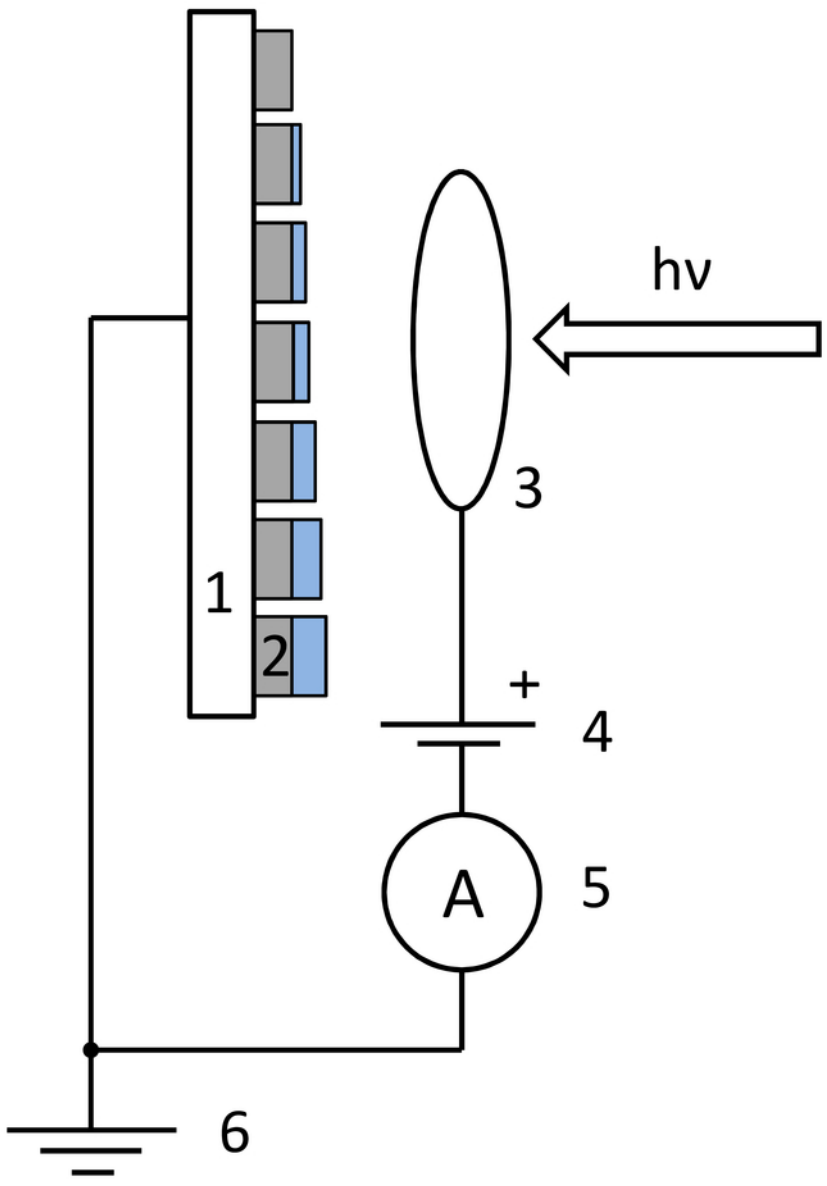
PLEASE CITE THIS ARTICLE AS DOI: 10.1063/1.50007163

Silicon wafer

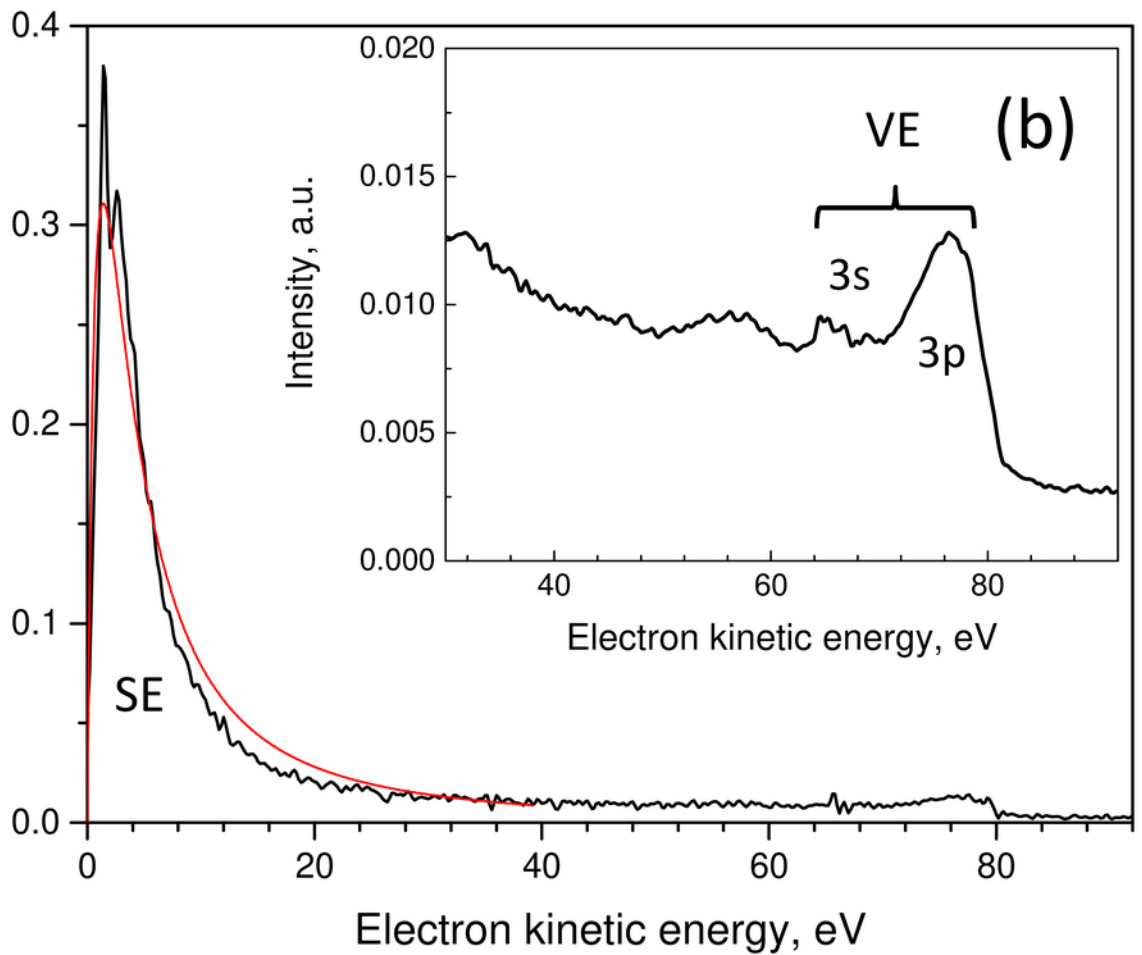
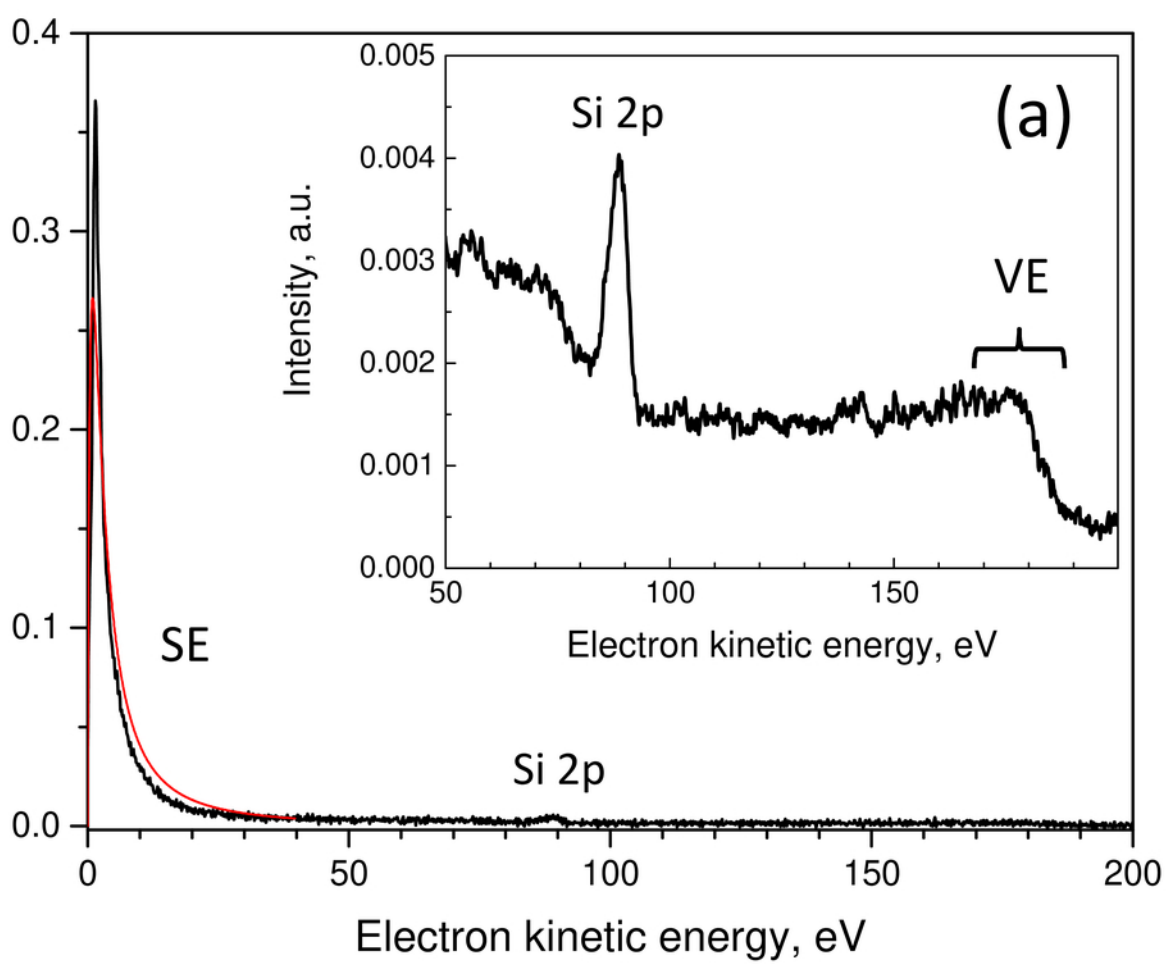
Polymer



This is the author's peer reviewed, accepted manuscript. However, the online version of record will be different from this version once it has been copyedited and typeset.
PLEASE CITE THIS ARTICLE AS DOI: 10.1063/5.0007163



This is the author's peer reviewed, accepted manuscript. However, the online version of record will be different from this version once it has been copyedited and typeset.
PLEASE CITE THIS ARTICLE AS DOI: 10.1063/5.0007163



This is the author's peer reviewed, accepted manuscript. However, the online version of record will be different from this version once it has been copyedited and typeset.
PLEASE CITE THIS ARTICLE AS DOI: 10.1063/5.0007163

